nature neuroscience

TECHNICAL REPORTS

Ultrafast optogenetic control

Lisa A Gunaydin[1,2,5], Ofer Yizhar[1,5], André Berndt[3,5], Vikaas S Sohal[1,4], Karl Deisseroth[1,4] & Peter Hegemann[3]

Channelrhodopsins such as channelrhodopsin-2 (ChR2) can drive spiking with millisecond precision in a wide variety of cells, tissues and animal species. However, several properties of this protein have limited the precision of optogenetic control. First, when ChR2 is expressed at high levels, extra spikes (for example, doublets) can occur in response to a single light pulse, with potential implications as doublets may be important for neural coding. Second, many cells cannot follow ChR2-driven spiking above the gamma (~40 Hz) range in sustained trains, preventing temporally stationary optogenetic access to a broad and important neural signaling band. Finally, rapid optically driven spike trains can result in plateau potentials of 10 mV or more, causing incidental upstates with information-processing implications. We designed and validated an engineered opsin gene (*ChETA*) that addresses all of these limitations (profoundly reducing extra spikes, eliminating plateau potentials and allowing temporally stationary, sustained spike trains up to at least 200 Hz).

Several microbial opsin genes encoding natural light-sensitive proteins have been adapted for neuroscience applications, allowing for millisecond-timescale optical control of neural activity[1,2]. Genomic discovery strategies have led to the identification of previously unknown opsins[2], and molecular engineering of opsin genes has not only optimized performance, but also has opened the door to new domains of functionality. For example, single amino acid alterations in the ChR2 sequence (C128) have generated a functionally distinct class of opsin genes, the step-function opsin (SFO) genes, encoding proteins that allow for bi-stable on-off switching of neural activity using only brief pulses of blue and green light[3]. The bi-stable switching property allows the sensitization of cells to native patterns of input without imposition of artificial spike trains and allows very long timescale experiments with minimal energy deposition into tissue, as light sensitivity and open-state stability are enhanced by several orders of magnitude. These studies underscore the potential effect that molecular engineering strategies may have on optogenetics, in this case by opening up new kinds of spike modulation and longer timescales to investigation.

On the other hand, major kinetic limitations of optogenetics still persist at short timescales, specifically in the poor access to high gamma and beyond (50–200 Hz), in artifactual extra spikes, and in membrane potential summation at high spike rates. Extra spikes were reported even in the initial study of channelrhodopsin optogenetics where comparatively low expression levels were achieved[4], and more modern techniques involving higher opsin expression levels have only exacerbated the problem (illustrated in **Fig. 1a**). However, spike failures are also a major issue; previously, we and others have reported that optical stimulation with ChR2 in excitatory neurons does not reliably evoke spikes at frequencies above the gamma (40 Hz) range[4–6]. Further complicating efforts to deliver precisely defined neural codes, these dropped spikes depend not only on light-pulse frequency, but also on light-pulse history with wild-type ChR2, as ChR2 recovery from inactivation is slow. Certain chimeras and mutations in opsin genes have led to improved conductance properties, but ~50% or more of light pulses result in spike failures when trains above 40 Hz are delivered[6–9]. The dropped spikes at these higher light-pulse rates are probably linked to ChR2 photocycle kinetics (light-induced inactivation resulting from accumulation of a late nonconducting photointermediate, P480)[10–12] and to host cell–specific properties of potassium and sodium channel activation/inactivation kinetics[13,14], but true spike frequency–response tests of ChR2 have been lacking because of the difficulty of targeting naturally fast-spiking cells[15,16]. Finally, the plateau potentials seen at high flash rates are presumably related to the 12-ms deactivation time constant of ChR2 interacting with endogenous cellular active conductances. Together, these kinetic considerations prevent the optical delivery of desired neural codes (in the broad frequency domain above 40 Hz) and lead to spurious triggering of undesirable signal confounds (both spike doublets and plateau-like states have intrinsic importance in neural processing). Therefore, we sought to engineer a channelrhodopsin that is compatible with minimal spike doublets and plateau potentials even at high expression levels and spike rates, and with the capability to drive precisely defined and sustained spike trains up to at least 200 Hz.

We considered that mutations or chimeras that simply increase expression, conductance or activation kinetics might improve the frequency response, but would not improve (and could well worsen) doublets and plateau potentials. However, it might be possible to resolve all three issues simultaneously by specifically accelerating channel deactivation gating via directed molecular engineering of ChR2 at amino acid residues that are thought to be critical for determining channel kinetics. Engineering faster off-kinetics for ChR2 could facilitate both higher frequency and more temporally precise optical stimulation, conferring the ability to optically mimic the full dynamic range of natural firing patterns without introducing artifacts. Predictions about the relevant protein residues were informed by sequence comparisons

[1]Department of Bioengineering, [2]Neuroscience Program, Stanford University, Stanford, California, USA. [3]Institute of Biology, Experimental Biophysics, Humboldt-University, Berlin, Germany. [4]Department of Psychiatry and Behavioral Sciences, Stanford University, Stanford, California, USA. [5]These authors contributed equally to this work. Correspondence should be addressed to P.H. (hegemape@rz.hu-berlin.de) or K.D. (deissero@stanford.edu).

Received 21 September 2009; accepted 4 January 2010; published online 17 January 2010; doi:10.1038/nn.2495

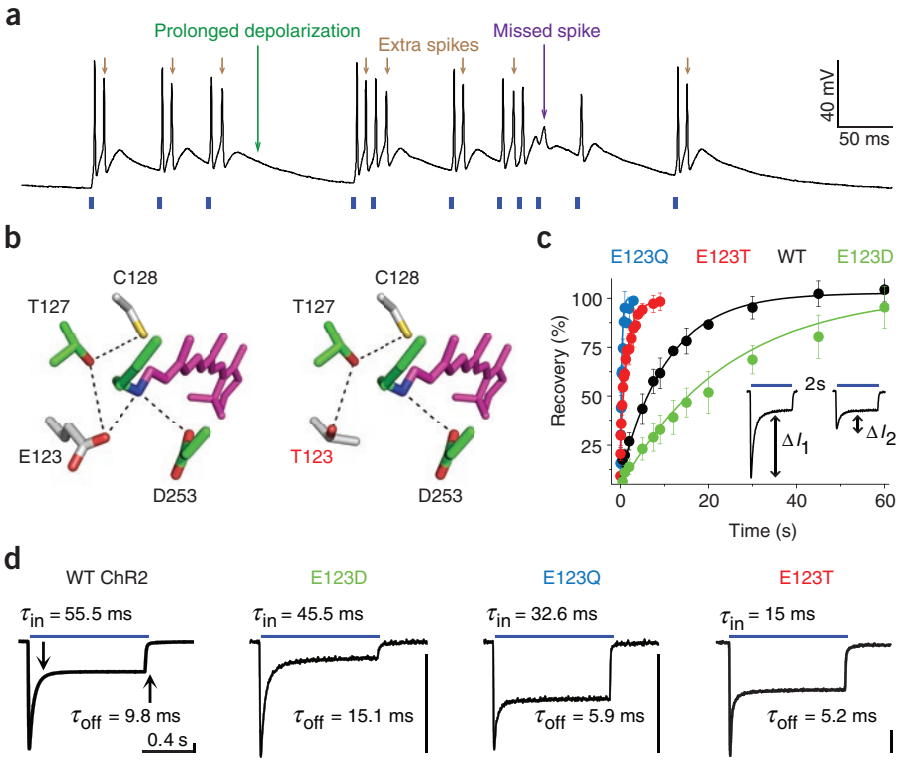

Figure 1 Rational design of a fast channelrhodopsin. (**a**) Whole-cell current-clamp recordings from a parvalbumin interneuron strongly expressing wild-type ChR2; note the extra spikes, the missed spike later in the train, and the prolonged depolarizations observed after termination of each 2-ms light pulse. (**b**) Left, homology model of ChR2 based on the bacteriorhodopsin X-ray structure (1KGB, RSCB protein data bank). The retinal is shown in violet, conserved residues in green and substitutions in ChR2 in gray. Oxygen is red, nitrogen is blue and sulfur is yellow. Right, formation of the complex RSB counterion was predicted to be disturbed by replacement of E123 with threonine (right). Candidate hydrogen bonds are shown as dotted lines. (**c**) Recovery of peak current in wild-type (WT) ChR2 and E123 mutants on stimulation with a second light pulse after a variable dark period, recorded in oocytes. Inset, peak recovery of wild-type ChR2 after 2 s in darkness at –75 mV in standard solution (100 mM NaCl, pH 7.5). The ratio of ΔI_2 to ΔI_1 yields the recovery in percent. Values for wild-type ChR2 (black), E123Q (blue), E123T (red) and E123D (green) are plotted versus the dark interval between the two flashes; data points were fit by a mono-exponential decay (colored lines). (**d**) Voltage-clamp recordings of wild-type ChR2, E123D, E123Q and E123T under stimulation with a 1-s light pulse (blue bars, 500 ± 25 nm, 50 mW cm^{-2}) at –100 mV and 100 mM NaCl in the external solution (pH 7.5). τ values characterize the mono-exponential transition from peak to stationary currents (τ_{in}) and current kinetics (τ_{off}) after the light was switched off. Vertical black bars represent 10 nA.

with the well-characterized bacterial proton pump bacteriorhodopsin, for which the crystal structure has been solved and in which point mutations have been shown to alter photocurrent kinetics. We therefore designed point mutations in the ChR2 sequence that would be predicted to accelerate channel closing to achieve rapid repolarization of neurons following a light pulse, and we validated our findings in both oocytes and neurons in intact mammalian brain tissue using a cell type–specific genetic targeting methodology[15–17].

RESULTS

Both extra spikes and persistent depolarizations can be observed on optical stimulation of cells that strongly express ChR2 (**Fig. 1a**). To eliminate unwanted spikes and promote rapid repolarization, we mutagenized ChR2 residues that are thought to be crucial for determining channel photocycle kinetics, employing a protein model based on the three-dimensional structure of bacteriorhodopsin. The most likely candidates for altering photocycle kinetics are the amino acid residues of the retinal binding pocket, particularly residues near the retinal Schiff base (RSB; **Fig. 1b**). In the dark state and in most other photocycle intermediates, the RSB is protonated (RSBH) and this protonated state is particularly stabilized by nearby carboxylic acids. In ChR2, the complex counterion is expected to be formed by E123 and D253 (homologous to D85 and D212 in bacteriorhodopsin) and indirectly by T127 and C128 (homologous to T89 and T90 in bacteriorhodopsin) (**Fig. 1b**). On light excitation of ChR2, the RSBH is briefly deprotonated and the channel transitions through a nonconducting P390 state before the conducting P520 state is reached[10,12]. We expected that modification of E123 would lead to destabilization of the counterion, a small red shift of the peak absorption wavelength and modification of the photocycle kinetics.

We replaced Glu123 by aspartic acid, glutamine and threonine, expressed the mutated channels in *Xenopus laevis* oocytes, and recorded light-induced currents. We first tested recovery kinetics in double pulse experiments (**Fig. 1c**), as faster recovery kinetics could lead to more temporally stationary responses in light pulse trains and the recovery kinetics of the transient peak after time in darkness is expected to correlate with inactivation kinetics[18,19]. We observed that the peak recovery was slower in the conservative E123D exchange ($\tau = 24.5 \pm 2.8$ s, $n = 6$, $P < 0.005$), whereas both E123T and E123Q recovered significantly faster ($\tau = 1 \pm 0.1$ s, $n = 6$, $P < 0.005$ and $\tau = 0.32 \pm 0.03$ s, $n = 4$, $P < 0.005$, respectively) than wild-type ChR2 ($\tau = 10.7 \pm 0.8$ s, $n = 15$) (at pH 7.5 and –75 mV; **Fig. 1c**). Examination of individual photocurrents (**Fig. 1d**) revealed that E123D exchange reduced the steady-state to peak-current ratio, whereas deactivation kinetics were slower ($\tau_{off} = 15.1 \pm 1.8$ ms, $n = 6$, $P < 0.005$) compared with those of wild-type ChR2 ($\tau_{off} = 9.8 \pm 1.3$ ms, $n = 10$; $pH_o = 7.5$, –100 mV). Replacement of Glu123 by glutamine gave rise to rapid, but weak, inactivation, and both of these mutations also caused a roughly tenfold reduction in photocurrent amplitude (via either reduced ChR2 expression or lower ion conductance), so we did not pursue them further (data not shown). The threonine at position 123 resembles the counterion complex of the light-driven chloride pump halorhodopsin[20], with diminished hydrogen-binding capability (**Fig. 1b**). On light stimulation, ChR2(E123T) showed increased steady state–to-peak current ratio and markedly faster off-kinetics ($\tau_{off} = 5.2 \pm 1.4$ ms, $n = 7$, $P < 0.005$) than wild-type ChR2, and, importantly, current amplitudes were larger than those for the other mutants (**Fig. 1d**).

We concluded that, for applications requiring fast gating kinetics combined with minimal inactivation and strong currents, the most promising mutant was ChR2(E123T). To study ChR2(E123T) in greater

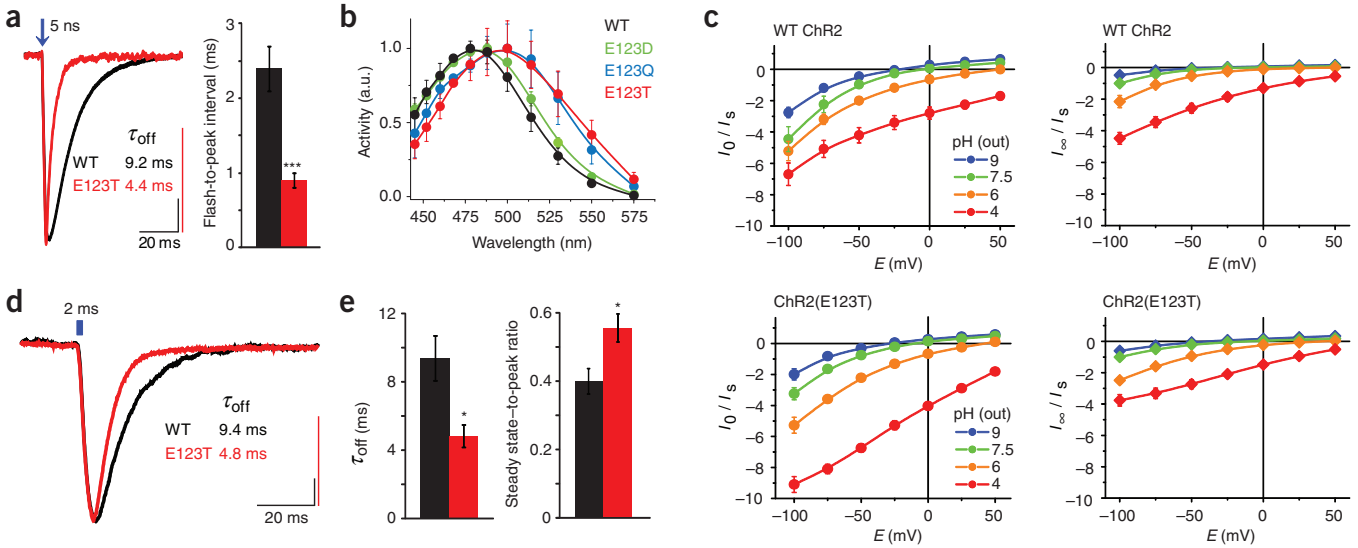

Figure 2 Photocurrent properties of E123T in oocytes and cultured neurons. (**a**) Oocyte current recordings. Excitation was delivered with a 5-ns laser flash (470 nm, 0.5 mW cm^{-2}, blue arrow) at –100 mV. Photocurrent decay was fitted mono-exponentially with τ values shown for wild-type ChR2 (black) and E123T (red) and traces were normalized to highlight differences in decay kinetics. Vertical bars correspond to 2.5 nA (wild type, black; E123T, red). (**b**) The action spectrum of E123T (red, $n = 6$) is shown in comparison with spectra of wild-type ChR2 (black, $n = 6$), E123D (green, $n = 3$) and E123Q (blue, $n = 4$). Current amplitudes were measured at the different wavelengths, normalized to respective maximum values and corrected for fluctuations of the flash intensity. (**c**) Current-voltage relationships of wild-type ChR2 and E123T at different external pH values in presence of 100 mM Na^+. Approximate current amplitudes at time zero (I_0, left) and steady state (I_∞, right) were normalized to the steady-state value for –100 mV at pH 7.5. Note that the pH dependence of the I_0 was larger for E123T. (**d**) Photocurrents evoked by 2-ms pulses of 470-nm light recorded from cultured hippocampal neurons expressing wild-type ChR2 (black) and ChR2(E123T) (red). Vertical bars correspond to 20 pA (wild type, black; E123T, red). (**e**) Left, summary of photocurrent amplitudes recorded as in **d**. Right, summary of steady state–to-peak current ratio recorded from cultured hippocampal neurons stimulated with 1-s, 470-nm light pulses at –70 mV.

detail, we conducted laser flash experiments, which confirmed the shorter lifetime of the conducting state ($\tau = 4.4 \pm 0.4$ ms ($n = 10$) and $\tau = 9.2 \pm 1.3$ ms ($n = 9$) for E123T and wild type, respectively; $P < 0.005$; **Fig. 2a**). We also were able to measure the flash-to-peak current time for ChR2(E123T) ($t_p = 0.9 \pm 0.1$ ms), which was more than twice as fast as that of wild-type ChR2 ($t_p = 2.4 \pm 0.3$ ms, $P < 0.005$). Also as predicted, laser excitation with varying wavelengths revealed a 20-nm red shift of the action spectrum for E123T compared with wild-type ChR2 (**Fig. 2b**), which may confer moderate benefit in terms of more effective tissue recruitment with deeper-penetrating green light. Finally, we measured the current-voltage relationship for peak and steady state currents I_0 and I_∞. We found that the pH dependence of I_0 was slightly stronger for E123T and inward rectification was less pronounced (**Fig. 2c**), reflecting a lower Na^+ conductance of the early open state[21]. However, the stationary current properties were quite similar in wild type and E123T, and at physiological pH the current-voltage relationships of wild type and E123T were nearly indistinguishable at both peak and steady state (**Fig. 2c**). We found that many of the advantageous properties of E123T were also conferred by a similar E123A mutation (**Supplementary Fig. 1**); however, of these two fast mutations, E123T may still be preferable because of its slightly larger currents and more red-shifted action spectrum (**Fig. 2b** and **Supplementary Fig. 1**).

As not all channelrhodopsins are expressed well in neurons, it was important to validate mutant expression in neuronal culture before *in vivo* translation. Given the promising properties of E123T, we created a lentiviral vector expressing ChR2(E123T) as an enhanced yellow fluorescent protein (EYFP) fusion protein driven by the *Camk2a* promoter, which we expressed in cultured hippocampal neurons. We found that this mutant was well expressed in neurons, with fast off-kinetics that closely matched those observed in oocytes ($\tau_{off} = 9.4 \pm 1.3$ ms and 4.8 ± 0.6 ms for wild type and E123T, respectively, $P < 0.05$; **Fig. 2d,e**). These kinetics for E123T were at least twofold faster than any channelrhodopsin reported to date. Moreover, although the currents were smaller (**Fig. 2a,d**), the steady state–to-peak current ratio increased by 40% compared with wild type, consistent with the decreased inactivation that we observed in oocytes (steady state:peak current ratio = 0.4 ± 0.04 and 0.6 ± 0.04 for wild type and E123T, respectively, $P < 0.05$, 1-s light pulse; **Fig. 2e**). We therefore designated fast kinetic mutants involving E123 as ChETA variants (from ChR2-E123T accelerated), a category that also includes E123A and combination mutants.

Although these properties appeared to represent a substantial step forward, it was crucial to quantify behavior not just in oocytes or slow pyramidal neurons, but also in cells capable of pushing the engineered channelrhodopsin to the limits of its performance. We therefore targeted a ChETA variant to cortical parvalbumin interneurons to characterize the limits of signal fidelity; in this case, E123T was introduced on an H134R background (which increases photocurrent amplitudes, but by itself slows off-kinetics[7,8]) to bring current size into the range of wild-type currents. We stereotactically injected a Cre-dependent adeno-associated viral vector carrying the opsin fusion genes (**Fig. 3a** and Online Methods) into transgenic mice expressing Cre recombinase under the control of the *parvalbumin* promoter (*Pvalb-cre* mice)[15,16], and obtained whole-cell recordings from targeted (YFP expressing) neurons in acute prefrontal brain slices. The mutant was robustly expressed in parvalbumin neurons (**Fig. 3b**) and exhibited a higher steady state–to-peak ratio than wild-type ChR2 in response to 1-s pulses of 470-nm blue light (**Fig. 3c**). Peak current amplitudes trended only slightly lower in the ChETA variant compared with wild type (848 ± 158 and 645 ± 47 pA in wild type and ChETA, respectively; $P = 0.26$, $n = 9$ wild-type and 8 ChETA cells; **Fig. 3c**) and faster off-kinetics were preserved indicating that E123T dominates the kinetics (**Fig. 3d**).

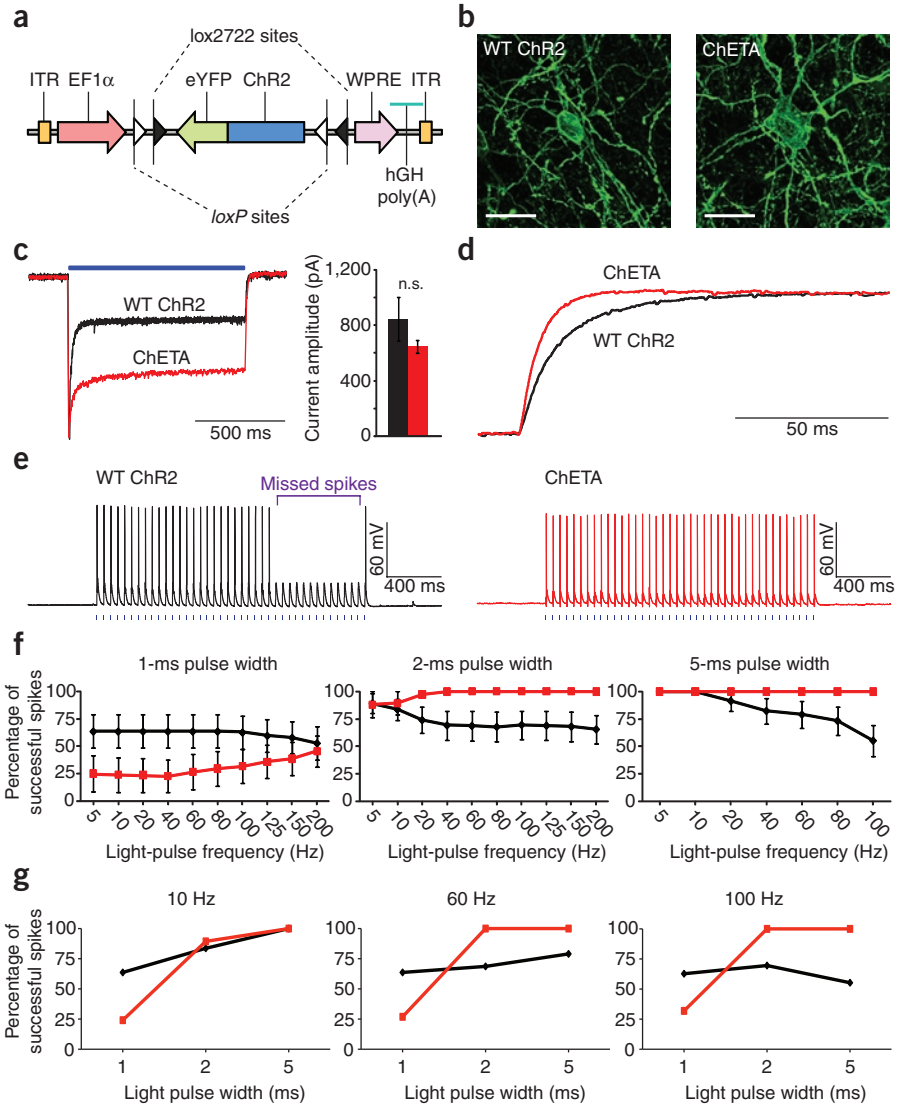

Figure 3 Frequency-response performance: spiking to 200 Hz. (**a**) Schematic of the adeno-associated virus (AAV) vector construct carrying a *loxP/lox2722*-flanked opsin gene. The resulting virus was injected into *Pvalb-cre* mice to achieve parvalbumin-specific opsin gene expression. (**b**) Confocal images of wild type (left) and ChETA (right) expression in prefrontal parvalbumin interneurons. Scale bars represent 20 μm. (**c**) Left, photocurrents evoked by a 1-s pulse of 472-nm blue light in prefrontal cortical parvalbumin interneurons. Traces are normalized to the peak photocurrent amplitude to illustrate the increase in the steady state–to-peak current ratio in ChETA (red) compared with wild-type ChR2 (black). Right, summary of steady-state current amplitudes in response to 1-s blue light pulses measured in parvalbumin interneurons that also expressed wild-type ChR2 (black) and ChETA (red), represented as mean ± s.e.m. ($n = 11$ and 8 for wild type and ChETA, respectively). (**d**) Expanded photocurrents from **c** normalized to steady-state current had accelerated off-kinetics in ChETA (red). (**e**) Whole-cell current-clamp recordings from parvalbumin interneurons that also expressed wild-type ChR2 (black) or ChETA (red) in response to 20-Hz light stimulation (472-nm, 2-ms pulse widths); note the higher percentage and temporal stationarity of successful spikes evoked with ChETA. (**f**) Summary of the percentage of successful spikes evoked over a range of light-pulse frequencies from 5–200 Hz in parvalbumin interneurons expressing wild-type ChR2 (black) or ChETA (red). (**g**) Summary of the percentage of successful spikes evoked with 1-, 2- and 5-ms light pulse widths, plotted at 10, 60 and 100 Hz from **e**. To determine whether light pulses were significantly more effective at eliciting spiking in ChETA-expressing cells than in wild-type ChR2-expressing cells, we computed the two-way ANOVA for each pulse width, comparing the percentage of successful spikes from many cells and using genotype (ChETA versus wild type) and frequency (5–200 Hz) as factors. We found a significant effect of genotype on the percentage of successful spikes fired, with ChETA outperforming wild-type ChR2 for both light-pulse widths ($P < 0.001$ for 2-ms and 5-ms pulse widths, $n = 11$ wild-type and 8 ChETA cells).

To test the utility of the ChETA variant, we stimulated cells with blue light-pulse trains over a range of light-pulse widths and over a range of frequencies from 5–200 Hz for each pulse width (**Fig. 3e**,**f**). As a result of spike failures, when we used light pulses that were 1 ms in duration, neither wild-type nor ChETA drove spiking reliably at any frequency (**Fig. 3f**); in fact, the ChETA underperformed wild-type ChR2 with these extremely brief light pulses, most likely because the ChETA was expected to generate reduced current per activated ChR during its shorter open time. But with a more typical 2-ms light pulse width, we found that the ChETA potently improved performance over a broad range of frequencies from 40–200 Hz, such that every light pulse reliably evoked an action potential, even in sustained 200-Hz trains (the highest frequency tested; **Fig. 3f**). In this regard, the ChETA considerably outperformed wild-type ChR2 (**Fig. 3f**) and a similar pattern was observed with 5-ms pulses (**Fig. 3f**); however, there was little advantage to using light pulses longer than 2 ms (**Fig. 3g**). With 2-ms light pulses, both wild-type ChR2 and the ChETA performed equally well at low frequencies (<20Hz), firing spikes in response to almost every light pulse, whereas, from 40 to 200 Hz, the ChETA substantially outperformed wild-type ChR2 (**Fig. 3g**). The ChETA also displayed marked temporal stationarity of efficacy (**Fig. 3e** and **Supplementary Fig. 2**), a feature that enables extended delivery of defined neural activity patterns. In contrast with wild-type ChR2, in which performance may deteriorate over long pulse trains, the ChETA's performance was stable during extended light pulse trains across a broad range of frequencies (5–200 Hz) and pulse widths (**Fig. 3e** and **Supplementary Fig. 2**). With this increased fidelity and by enabling control of neural spiking in intact mammalian brain tissue up to at least 200 Hz, channelrhodopsins engineered in this way fill a distinct need that is not addressed by existing technology.

High-fidelity optogenetics requires not only reliable elicitation of evoked signals, as shown above, but also minimization of spurious signals. Our strategy for opsin engineering was chosen to minimize extra spikes and plateau potentials. We therefore compared the ChETA and wild-type ChR2 with regard to artifactual signal generation. We found that parvalbumin-positive neurons expressing wild-type ChR2 at high levels could fire spike doublets and triplets in response to 2-ms light pulses (**Fig. 4a**), even while following and generating output power at the desired frequency, and generated plateau potentials at high frequencies, as the cells were unable

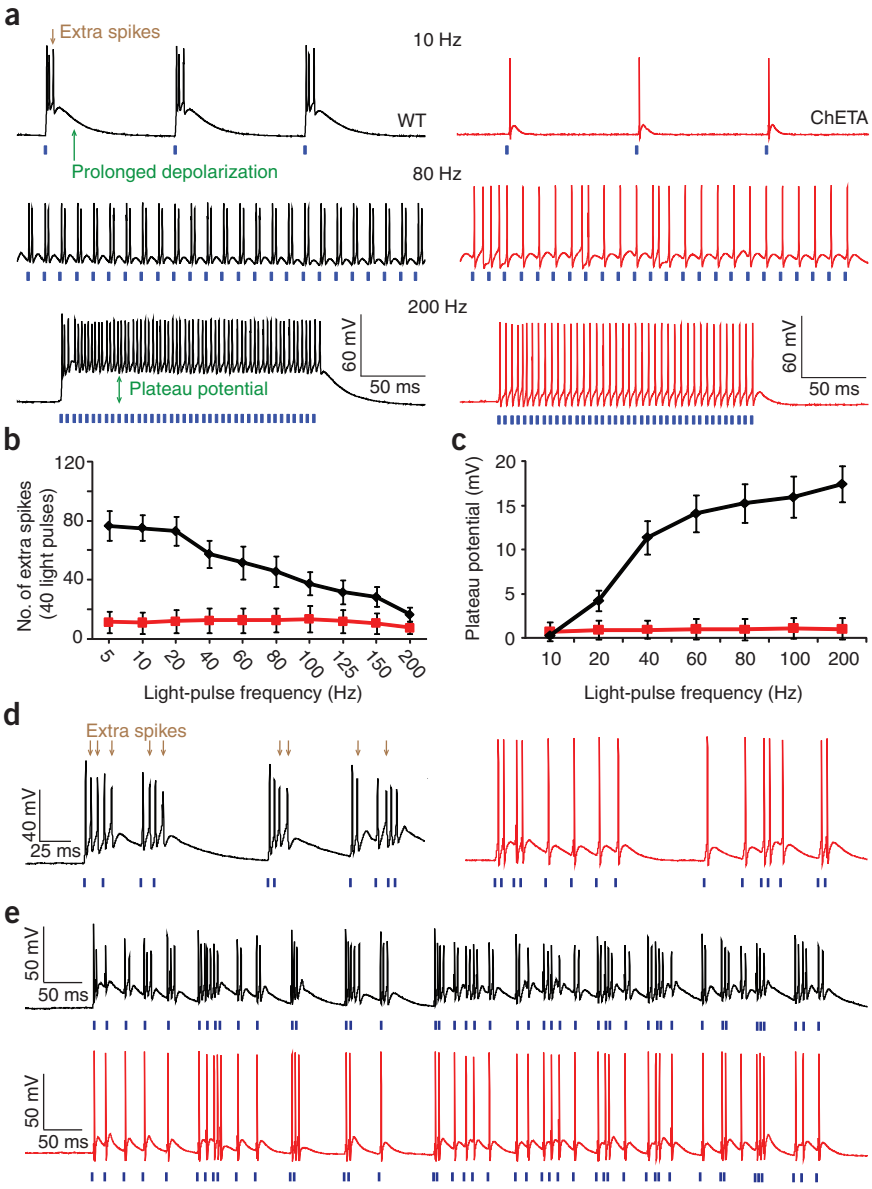

Figure 4 Multiple dimensions of enhanced ChETA performance. (**a**) Whole-cell current-clamp recordings from parvalbumin interneurons expressing wild-type ChR2 (black) or ChETA (red) in response to 10-, 80- and 200-Hz light stimulation (rows 1, 2 and 3, respectively; all 472-nm, 2-ms light pulse widths). Note the brisker repolarizations and reduced extra spikes in ChETA-expressing interneurons. Scale bars apply to all traces. (**b**) Summary of extra spikes evoked by trains of 2-ms light pulses (total of 40 pulses) in parvalbumin interneurons expressing wild-type ChR2 (black) or ChETA (red), data averaged from cells that spiked to 100% to light pulses ranging from 5–200Hz ($n = 5$ and 7 for wild type and ChETA, respectively). (**c**) Summary of plateau potential amplitude in parvalbumin neurons that also expressed wild-type ChR2 or ChETA, measured from baseline to the trough between light pulses in the middle of the train (2-ms light pulses). (**d**) Spike waveforms in interneurons expressing wild-type ChR2 (black) and ChETA (red) evoked by Poisson pulse trains consisting of 2-ms light pulses delivered at a mean rate of 40 Hz. Traces were chosen to match the resting membrane potential. Arrows denote extra spikes. Scale bars apply to both traces. (**e**) Responses of interneurons expressing wild-type ChR2 (black) and ChETA (red) to extended Poisson pulse trains with the same parameters as in **c**; note the reduced extra spikes, larger spike amplitudes and rapid repolarization.

to adequately repolarize between light pulses (**Fig. 4a**). In marked contrast, with the same 2-ms light pulses, ChETA-expressing cells responded with far fewer extra spikes across all frequencies of stimulation ($P < 0.001$, two-way ANOVA; **Fig. 4a**,**b**). Notably, the ChETA also abolished plateau potentials across all frequencies, even as the cells followed light pulses reliably and precisely (**Fig. 4a**,**c**) up to 200 Hz. Similarly enhanced ChETA performance was seen with more naturalistic input patterns, using pseudo-random Poisson trains of light flashes (mean rate of 40 Hz; **Fig. 4d**). As with rhythmic light trains, extra spikes (**Fig. 4d**) were virtually abolished in the ChETA-mediated responses. Larger spike amplitudes and more robust after-hyperpolarizations were also seen using ChETA compared with wild-type ChR2 (**Fig. 4d**); these properties were born out even over long, naturalistic Poisson trains (**Fig. 4e**), highlighting the reduced desensitization of active conductances expected from brisker repolarization and elimination of spurious spike multiplets.

DISCUSSION

We found that rational molecular engineering of the Schiff-base counterion environment in a channelrhodopsin resulted in profoundly accelerated deactivation kinetics. When delivered as an optogenetic tool to intact mammalian brain tissue, the channelrhodopsin caused a reduction in the number of spurious light-evoked spikes, complete elimination of artifactual plateau potentials, increased temporal stationarity, and precisely timed and sustained spike trains up to at least 200 Hz.

Structural considerations are of interest in understanding the performance of this engineered channelrhodopsin. Threonine at the counterion position might have been expected to lower the RSB/RSBH pK, as is the case in bacteriorhodopsin (for which the D85T mutation shifts the pK from 13 to 8.7)[22], which would cause the RSB to deprotonate near physiological or high pH. However, this deprotonation apparently does not occur with E123T, which is fully active up to pH 9 (**Fig. 2c**). It is also interesting that the current-voltage relation was altered for the E123T peak current, but not the steady-state current, and even for peak current the relationship was altered only at extreme pH (4.0; **Fig. 2c**). Finally, we found that the ratio of peak to steady-state current was essentially pH independent for E123T, whereas the ratio increased with pH for wild type. This may be understood by considering that ChRs can exist in two open states, O1 and O2, which are populated with different proclivity from the dark-adapted and light-adapted states D470 and P480, respectively; O1 carries most of the peak current, whereas O2 is more prominent in the steady-state current and is twofold less Na^+ selective than O1 (ref. 21). The smaller peak-to–steady state ratio of E123T at high pH compared with wild type, and consequently lower degree of inactivation (pH 7.5 or 9; **Fig. 2c**), could represent a reduced preference of O1 for Na^+ compared with O2.

However, additional work will be required to assess this possible mechanism and to rule out an accelerated transition from O1 to O2 in E123T at acidic pH.

With regard to optogenetics application considerations, we note that it will be important to validate the optimal light-pulse parameters in each experimental preparation; although we have found that driving a ChETA with 2-ms light pulses elicited the most reliable and precise responses in cortical parvalbumin neurons, shorter or longer pulse widths may be optimal in other cell types or with different expression systems. It is also important to consider for each preparation the degree to which an engineered opsin will be helpful; there could be cases in which ChETA usage does not confer major advantages. The frequency response of a cell will ultimately be controlled by intrinsic cellular biophysical properties (for example, most pyramidal cells do not follow well beyond 40 Hz even with current injection) and not just by the properties of the introduced channelrhodopsin. However, we note that there is little downside to the use of ChETA variants apart from a slight reduction in peak current amplitude. In contrast, the H134R ChR2 single mutant used in previous optogenetic studies of parvalbumin neurons[16], which has increased current size but slower channel off-kinetics, results in reliable low-frequency spiking, but a much steeper drop-off in spike reliability at high frequencies beyond the gamma band.

The potential value of ChETA variants extends beyond high-frequency spiking, as the reduction in spurious extra spikes and plateau potentials will reduce confounds for experimental interpretations across stimulation frequencies (for example, roles for spike multiplets have been suggested in synaptic plasticity[23], long-range gamma synchrony between distant brain regions[24] and seizure propagation[25]). Moreover, ChETA responses were less variable and more stationary under stimulation frequencies (>40 Hz) that pushed kinetic limits so that the channels bordered on inactivation, as the recovery of peak current was much faster for the ChETA variant (**Fig. 1**), thereby enabling rapid recovery between high-frequency light pulses and ensuring more reliable responses from cell-to-cell and across extended trains.

Together, the properties conferred by ChETAs open the door to optical stimulation at and beyond the gamma band, up to at least 200 Hz, enabling truly versatile optogenetic control. ChETAs achieve this goal while improving temporal stationarity and virtually eliminating plateau potentials and extra spikes, thereby improving the precision of optogenetics even at lower frequencies. Rationally designed, molecularly engineered channelrhodopsins may continue to enable new dimensions of experimental control in the study of normal and pathological excitable cell function in intact biological systems.

METHODS

Methods and any associated references are available in the online version of the paper at http://www.nature.com/natureneuroscience/.

Note: Supplementary information is available on the Nature Neuroscience website.

ACKNOWLEDGMENTS

L.A.G. is supported by a BioX fellowship from Stanford University, O.Y. by an Human Frontier Science Program fellowship, and V.S.S. by a K99 Award from the US National Institutes of Health. A.B. is supported by a Leibniz Graduate School fellowship. P.H. is supported by the Deutsche Forschungsgemeinschaft (HE3824/9 and Cluster of Excellence: Unifying concepts in Catalysis). K.D. is supported by the William M. Keck Foundation, the Snyder Foundation, the Albert Yu and Mary Bechmann Foundation, the Wallace Coulter Foundation, the California Institute for Regenerative Medicine, the McKnight Foundation, the Esther A. and Joseph Klingenstein Fund, the National Science Foundation, the National Institute of Mental Health, the National Institute on Drug Abuse, and a US National Institutes of Health Pioneer Award.

AUTHOR CONTRIBUTIONS

All authors conceived and designed the experiments. L.A.G., O.Y., A.B. and V.S.S. conducted the experiments and contributed to the writing and analysis. K.D. and P.H. contributed to the writing and analysis, and supervised all aspects of the work.

COMPETING INTERESTS STATEMENT

The authors declare no competing financial interests.

Published online at http://www.nature.com/natureneuroscience/.
Reprints and permissions information is available online at http://www.nature.com/reprintsandpermissions/.

1. Zhang, F., Aravanis, A.M., Adamantidis, A., de Lecea, L. & Deisseroth, K. Circuit-breakers: optical technologies for probing neural signals and systems. *Nat. Rev. Neurosci.* **8**, 577–581 (2007).
2. Zhang, F. *et al.* Red-shifted optogenetic excitation: a tool for fast neural control derived from *Volvox carteri*. *Nat. Neurosci.* **11**, 631–633 (2008).
3. Berndt, A., Yizhar, O., Gunaydin, L.A., Hegemann, P. & Deisseroth, K. Bi-stable neural state switches. *Nat. Neurosci.* **12**, 229–234 (2009).
4. Boyden, E.S., Zhang, F., Bamberg, E., Nagel, G. & Deisseroth, K. Millisecond-timescale, genetically targeted optical control of neural activity. *Nat. Neurosci.* **8**, 1263–1268 (2005).
5. Ishizuka, T., Kakuda, M., Araki, R. & Yawo, H. Kinetic evaluation of photosensitivity in genetically engineered neurons expressing green algae light-gated channels. *Neurosci. Res.* **54**, 85–94 (2006).
6. Lin, J.Y., Lin, M.Z., Steinbach, P. & Tsien, R.Y. Characterization of engineered channelrhodopsin variants with improved properties and kinetics. *Biophys. J.* **96**, 1803–1814 (2009).
7. Nagel, G. *et al.* Light activation of channelrhodopsin-2 in excitable cells of *Caenorhabditis elegans* triggers rapid behavioral responses. *Curr. Biol.* **15**, 2279–2284 (2005).
8. Gradinaru, V. *et al.* Targeting and readout strategies for fast optical neural control *in vitro* and *in vivo*. *J. Neurosci.* **27**, 14231–14238 (2007).
9. Wang, H. *et al.* Molecular determinants differentiating photocurrent properties of two channelrhodopsins from chlamydomonas. *J. Biol. Chem.* **284**, 5685–5696 (2009).
10. Ernst, O.P. *et al.* Photoactivation of channelrhodopsin. *J. Biol. Chem.* **283**, 1637–1643 (2008).
11. Bamann, C., Kirsch, T., Nagel, G. & Bamberg, E. Spectral characteristics of the photocycle of channelrhodopsin-2 and its implication for channel function. *J. Mol. Biol.* **375**, 686–694 (2008).
12. Ritter, E., Stehfest, K., Berndt, A., Hegemann, P. & Bartl, F.J. Monitoring light-induced structural changes of Channelrhodopsin-2 by UV-visible and Fourier transform infrared spectroscopy. *J. Biol. Chem.* **283**, 35033–35041 (2008).
13. Mainen, Z.F., Joerges, J., Huguenard, J.R. & Sejnowski, T.J. A model of spike initiation in neocortical pyramidal neurons. *Neuron* **15**, 1427–1439 (1995).
14. Huguenard, J.R. & McCormick, D.A. Simulation of the currents involved in rhythmic oscillations in thalamic relay neurons. *J. Neurophysiol.* **68**, 1373–1383 (1992).
15. Sohal, V.S., Zhang, F., Yizhar, O. & Deisseroth, K. Parvalbumin neurons and gamma rhythms enhance cortical circuit performance. *Nature* **459**, 698–702 (2009).
16. Cardin, J.A. *et al.* Driving fast-spiking cells induces gamma rhythm and controls sensory responses. *Nature* **459**, 663–667 (2009).
17. Tsai, H.C. *et al.* Phasic firing in dopaminergic neurons is sufficient for behavioral conditioning. *Science* **324**, 1080–1084 (2009).
18. Nagel, G. *et al.* Channelrhodopsin-2, a directly light-gated cation-selective membrane channel. *Proc. Natl. Acad. Sci. USA* **100**, 13940–13945 (2003).
19. Hegemann, P., Ehlenbeck, S. & Gradmann, D. Multiple photocycles of channelrhodopsin. *Biophys. J.* **89**, 3911–3918 (2005).
20. Kolbe, M., Besir, H., Essen, L.O. & Oesterhelt, D. Structure of the light-driven chloride pump halorhodopsin at 1.8 A resolution. *Science* **288**, 1390–1396 (2000).
21. Berndt, A., Prigge, M., Gradmann, D. & Hegemann, P. Two open states with progressive proton selectivities in the branched channelrhodopsin-2 photocycle. *Biophys. J.* (in the press) (2010).
22. Tittor, J., Schweiger, U., Oesterhelt, D. & Bamberg, E. Inversion of proton translocation in bacteriorhodopsin mutants D85N, D85T, and D85,96N. *Biophys. J.* **67**, 1682–1690 (1994).
23. Lisman, J.E. Bursts as a unit of neural information: making unreliable synapses reliable. *Trends Neurosci.* **20**, 38–43 (1997).
24. Traub, R.D., Whittington, M.A., Stanford, I.M. & Jefferys, J.G. A mechanism for generation of long-range synchronous fast oscillations in the cortex. *Nature* **383**, 621–624 (1996).
25. Lévesque, M. *et al.* Synchronized gamma oscillations (30–50 Hz) in the amygdalo-hippocampal network in relation with seizure propagation and severity. *Neurobiol. Dis.* **35**, 209–218 (2009).

ONLINE METHODS

All experiments were conducted under protocols approved by the Stanford Administrative Panel on Laboratory Animal Care.

Homology model of bacteriorhodopsin. The chromophore model in **Figure 1b** is based on the dark state structure of bacteriorhodopsin (1KGB), as described previously[26]. Replacement of amino acid residues was done using MacPyMOL (DeLano Scientific LLC, http://www.csb.yale.edu).

Expression and electrophysiology of ChR2 mutants in *Xenopus laevis* oocytes. Wild-type ChR2 DNA (residues 1–315) was cloned into pGEM-HE vector and single bases were replaced by Quick Change mutagenesis kit (Stratagene) to obtain ChR2 mutants. Plasmids were transcribed by T7 RNA polymerase (Ambion). We injected 20 ng of mRNA into *Xenopus laevis* oocytes (Ecocyte) and incubated them for 3–7 d in Ringer solution (96 mM NaCl, 5 mM KCl, 2 mM $CaCl_2$, 1 mM $MgCl_2$ and 5 mM MOPS, pH 7.5) with streptomycin (1 mg ml^{-1}), penicillin (1 mg ml^{-1}) and all-trans-retinal (1 μM). Current recordings were performed with a GeneClamp 500 voltage-clamp amplifier (Axon) at sampling rates between 10 and 250 kHz. For recordings under continuous light conditions, oocytes were excited by a 75-W Xenon lamp (Osram) and wavelengths were adjusted by broad band interference filters (K-series Balzer). We provided 10-ns laser flashes with wavelengths between 400 and 600 nm by an adjustable Rainbow OPO (Opotek), pumped by Brillant b Nd:YAG-Laser (Quantel) to record fast kinetics and action spectra. The external solution contained 100 mM NaCl, 0.1 mM $CaCl_2$, 1 mM $MgCl_2$ and 5 mM MOPS (pH 7.5) or 5 mM glycine (pH 9) or 5 mM citrate (pH 6.4). To determine the ChR2 cation selectivity, we replaced Na^+ with 100 mM NMG^+.

Hippocampal neuron culture. Hippocampi were isolated from postnatal day 0 Sprague-Dawley rats (Charles River) and treated with papain (20 U ml^{-1}) for 45 min at 37 °C. The digestion was stopped with 10 ml of MEM/Earle's salts, without L-glutamine, and with 20 mM glucose, Serum Extender (1:1,000), and 10% heat-inactivated fetal bovine serum (vol/vol) containing 25 mg of bovine serum albumin and 25 mg of trypsin inhibitor. The tissue was triturated in a small volume of this solution with a fire-polished Pasteur pipette and ~100,000 cells in 1 ml were plated per coverslip in 24-well plates. Glass coverslips (prewashed overnight in HCl followed by several 100% ethanol washes and flame sterilization) were coated overnight at 37 °C with 1:50 Matrigel (Collaborative Biomedical Products). Cells were plated in culture medium, Neurobasal containing 2× B-27 (Life Technologies) and 2 mM Glutamax-I (Life Technologies). Half of the medium was replaced with culture medium the next day, giving a final serum concentration of 1.75%. No all-trans-retinal was added to the culture medium or recording medium for any of the neuronal experiments described here.

Construction of viral expression vectors. The plasmid encoding ChR2(E123T)-YFP was constructed by site-directed mutagenesis (Quikchange, Invitrogen) of the pLenti-CaMKIIa-ChR2-EYFP-WPRE vector, as previously described. Briefly, a PCR reaction was carried out using the above plasmid as template. High-performance liquid chromatography–purified primers (Operon Technologies) were used to introduce the mutated bases. The primer sequences for E123T were CAG TGG CTG CGC TAT GCA ACC TGG CTG CTC ACT TGT CC (sense) and GGA CAA GTG AGC AGC CAG GTT GCA TAG CGC AGC CAC TG (antisense). All mutations were then confirmed by DNA sequencing. VSVg-pseudotyped recombinant lentiviruses were produced as previously described (detailed at http://www.stanford.edu/group/dlab/optogenetics/expression_systems) by triple-transfection of HEK 293FT cells (Invitrogen) with pLenti-CaMKIIa-ChR2-EYFP-WPRE or the mutated plasmid, pVSVg, and pCMVdeltaR8.7. Virus supernatant was collected 40 h after transfection and applied to neurons.

For expression of wild-type ChR2 and ChR2(E123T) in fast-spiking neurons, we subcloned from the lentiviral vectors into a *loxP/lox2722*-flanked, inverted ORF plasmid (pAAV-EF1α-DIO-ChR2-YFP-WPRE[2]) that was only expressed in cells that coexpress Cre recombinase. E123T was inserted on the H134R background (which increases photocurrent amplitudes, but by itself slows off-kinetics) to bring current size in the range of wild-type currents. AAV virus was produced by the University of North Carolina Chapel Hill Vector Core at a titer of 3.0×10^{12} cfu ml^{-1}. We injected 1 μl of virus suspension stereotactically into the brains of 3–5-week-old mice. Coordinates for prefrontal cortex were +1.7 anteroposterior, 0.4 mediolateral and 2.5 dorsoventral (in mm from bregma).

Electrophysiological recordings in mammalian neurons. For whole-cell recording in cultured hippocampal neurons, the intracellular solution contained 129 mM potassium gluconate, 10 mM HEPES, 10 mM KCl, 4 mM MgATP and 0.3 mM Na_3GTP, titrated to pH 7.2. Tyrode's solution was employed as the extracellular solution (125 mM NaCl, 2 mM KCl, 2 mM $CaCl_2$, 1 mM $MgCl_2$, 30 mM glucose and 25 mM HEPES, titrated to pH 7.4). Recordings were conducted on an upright Leica DM-LFSA microscope equipped with a 40× water-immersion objective. Borosilicate glass (Sutter Instruments) pipette resistances were ~5 MΩ, with a range of 4–6 MΩ. Access resistance was 10–30 MΩ and was monitored for stability throughout the recording. Tyrode's solution was constantly perfused at a rate of 2 ml min^{-1} and heated to maintain a bath temperature of 32.5 ± 1°. Voltage-clamp recordings were carried out in Tyrode's solution containing 1 μM tetrodotoxin. Current-clamp recordings were conducted in the presence of the synaptic transmission blockers 6-cyano-7-nitroquinoxaline-2,3-dione (10 μM), D(–)-2-amino-5-phosphonovaleric acid (25 μM) and gabazine (10 μM) (Sigma). Photocurrents were evoked using a Lambda DG-4 optical switch (Sutter Instruments) with a 300-W xenon lamp and a 470-nm (HQ470/40) bandpass filter (Chroma). Light power at the specimen was 1.4 mW mm^{-2}. Patch-clamp recordings in slices from *Pvalb-cre* transgenic mice were conducted 2–3 weeks after virus injection. Recordings were carried out as described previously[27] and light delivery was similar to that used for cultured cells. Fast-spiking cells were identified by their expression of YFP and confirmed by their unique electrophysiological properties, that is, short action potentials (half-width < 0.5 ms) and rapid (>200 Hz), non-accommodating firing in response to depolarizing current pulses. Cell health and access resistance were continuously monitored throughout the experiment and cells were discarded if their resting potential was unstable or depolarized above –60 mV. In addition to purely rhythmic trains of light flashes, we also stimulated neurons using pseudorandom trains of light flashes with a Poisson distribution of interflash intervals. To generate a Poisson train with a mean rate of 40 Hz, we divided each sweep into 5-ms bins and assumed that the probability of a light flash occurring during each bin was 0.1.

Statistics and data analysis. Data was analyzed using Clampfit software (Axon Instruments) and custom software written in MATLAB (Mathworks). Statistical analysis was performed using Microsoft Excel (for *t* tests) and MATLAB (for ANOVAs).

26. Berndt, A., Yizhar, O., Gunaydin, L.A., Hegemann, P. & Deisseroth, K. Bi-stable neural state switches. *Nat. Neurosci.* **12**, 229–234 (2009).
27. Sohal, V.S., Zhang, F., Yizhar, O. & Deisseroth, K. Parvalbumin neurons and gamma rhythms enhance cortical circuit performance. *Nature* **459**, 698–702 (2009).

doi:10:1038/nn.2495